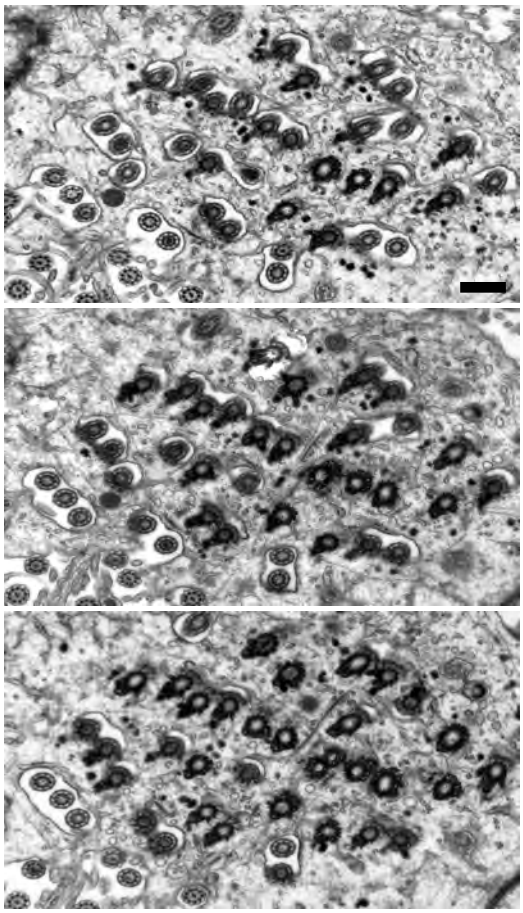

Figure S1. 3 sequential electron micrographs from a serially reconstructed ependymal cell in region AD. Note the consistency of basal foot orientation with the direction of CSF flow (anteroventral flow corresponding to leftward and downward in these images). Scale bar = 0.5 um.

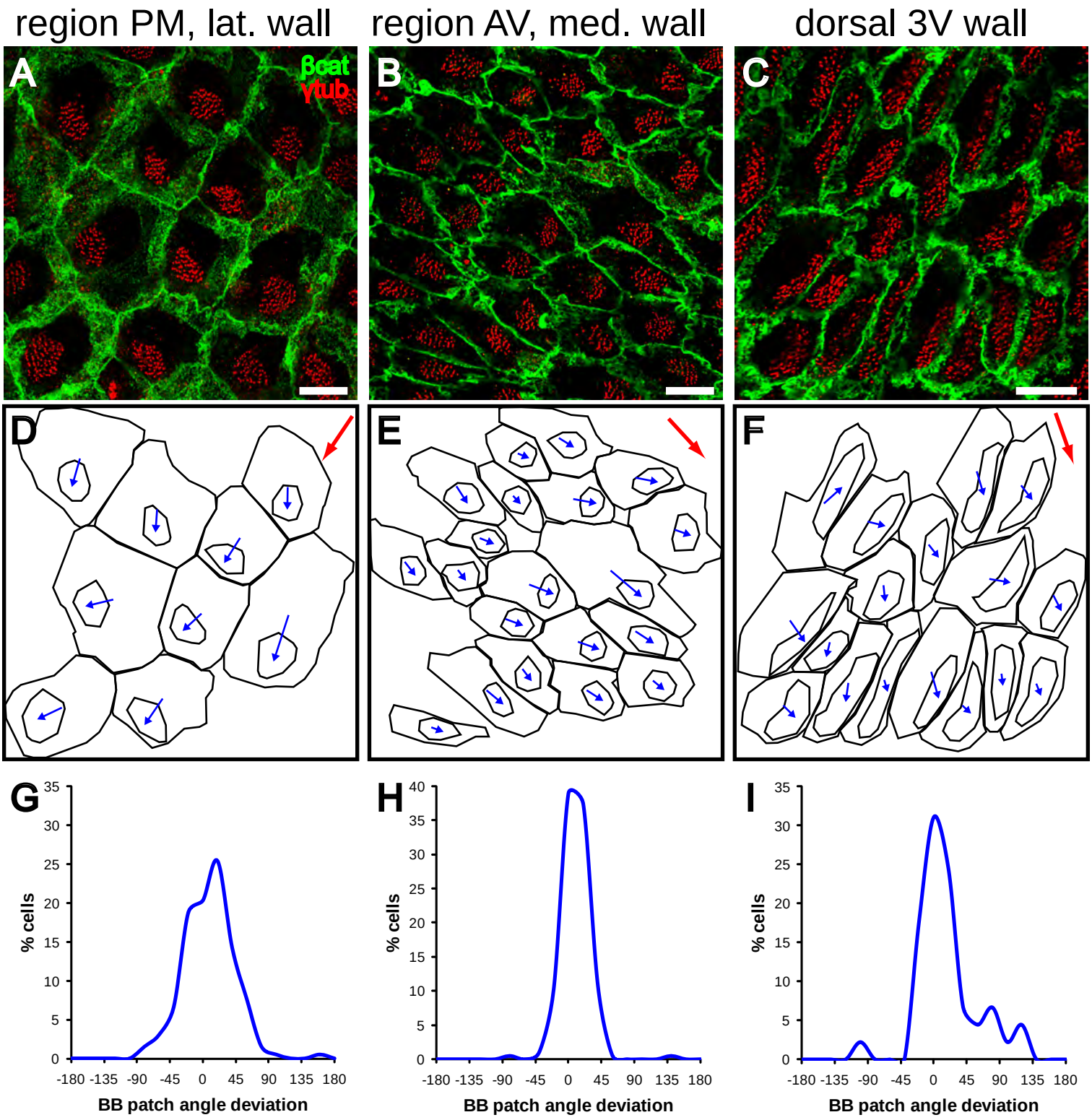

Figure S2. Basal body patch position is a cellular indicator of ependymal planar polarity throughout the adult ventricular system. **(A-C)** Confocal images of ventricular surfaces stained for β-catenin (green) and γ-tubulin (red). Scale bar = 10 um. **(A)** Region PM of the lateral wall of the LV (see Fig. 1A). **(B)** Region AV of the medial wall of the LV (see flow in supplemental Fig. S3). Region AV of the medial wall is directly across the ventricular cavity from region AV of the lateral wall; flow across these two regions is similarly oriented. **(C)** Dorsal 3rd ventricle wall. **(D-F)** Traces of the apical surfaces and basal body patches in (A-C), with vectors indicating the relative position of the BB patch. The red arrows indicate the direction of the median angle in each region. **(G-I)** Histograms showing the narrow distribution of BB patch angles around the median in regions shown above.

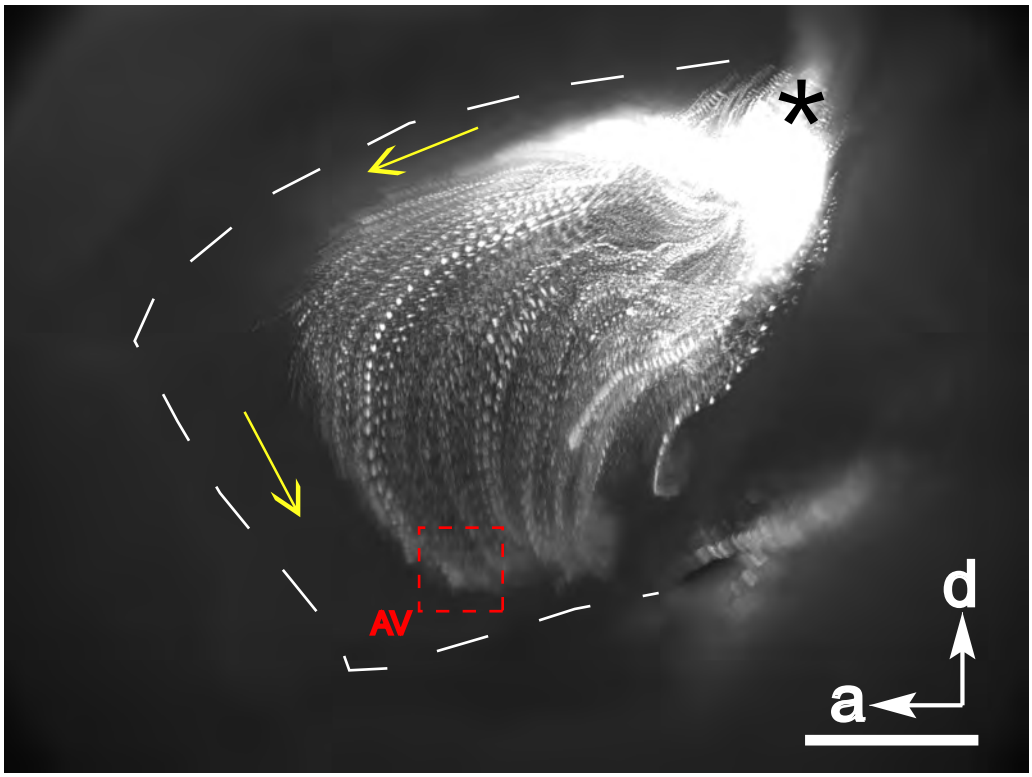

Figure S3. Orientation of fluid flow on the anterior medial wall of the LV. This image represents 30 frames of a movie were merged into a single picture. To make this movie, beads were deposited (*) on the surface of a wholemount of the anterior medial wall of the lateral ventricle. Planar polarized beating of ependymal cilia on the wholemount surface is indirectly visualized by oriented flow lines of fluorescent (2 um) microbeads. Within a line, the position of an individual bead is seen in consecutive frames. Yellow arrows indicate direction of flow. Red box indicates region AV of the medial wall, which is shown in Fig. S2B. Note that the orientation of flow shown here corresponds to that on the anterior lateral wall (Fig. 1A). Anterior (a) and dorsal (d) directions are indicated by arrows in the lower right corner. Scale bar = 0.5 mm.

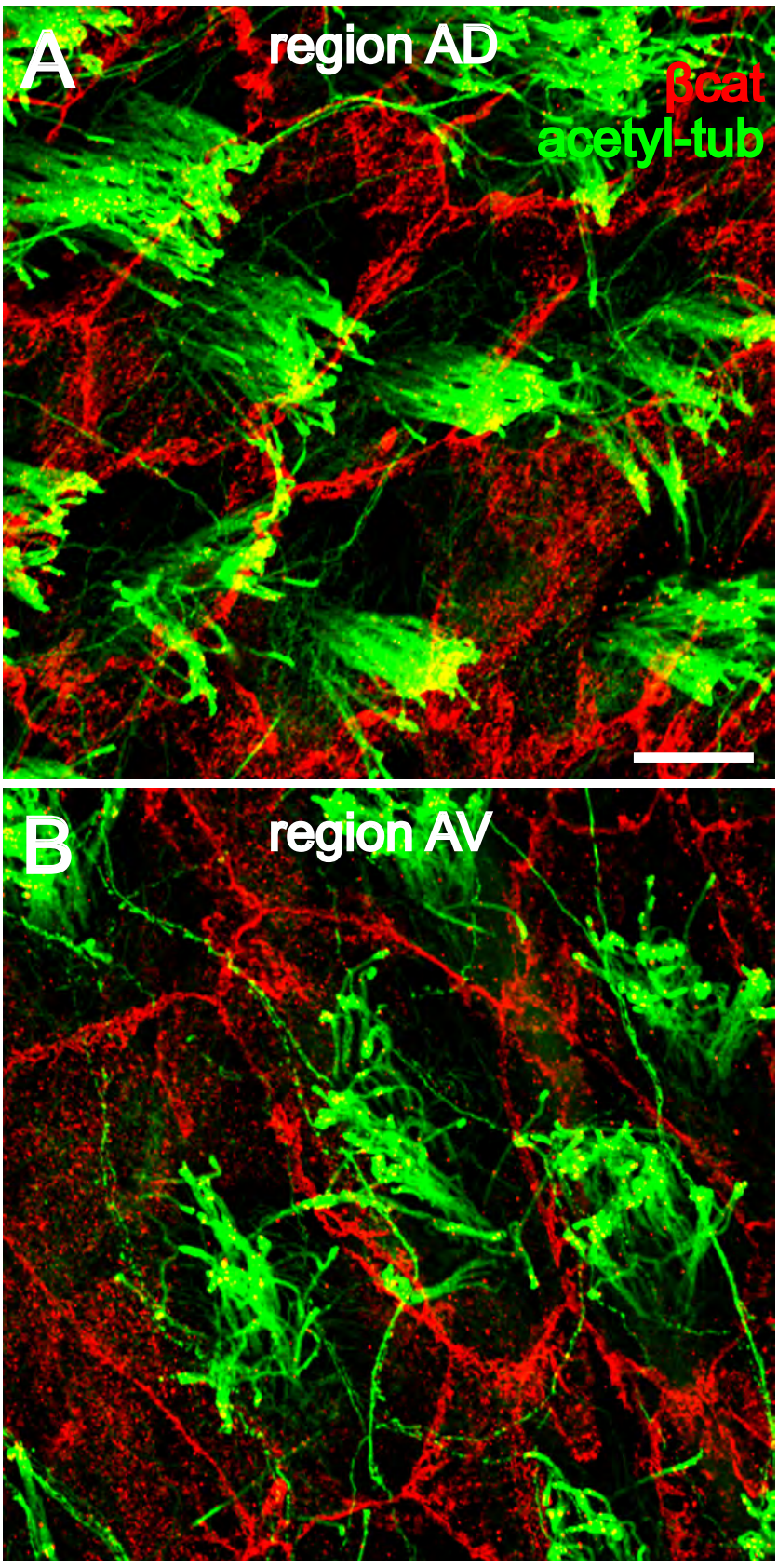

Figure S4. En-face confocal images of lateral wall wholemounts stained for acetylated tubulin (green) and β-catenin (red) confirmed that ciliary bundles emanate from one side of the ependymal cell's apical surface, consistent with the localization of basal bodies. In both region AD and AV, the ciliary bundles are displaced to the "downstream" side of the apical surface with respect to CSF flow. In addition, note that it would be impossible to determine planar orientation in fixed tissue based on ciliary form alone (acetylated tubulin staining without β-catenin). Although during active beating, the cilia have polarized bending forms, these oriented forms are not maintained invariantly during tissue fixation. Scale bar = 10 um.

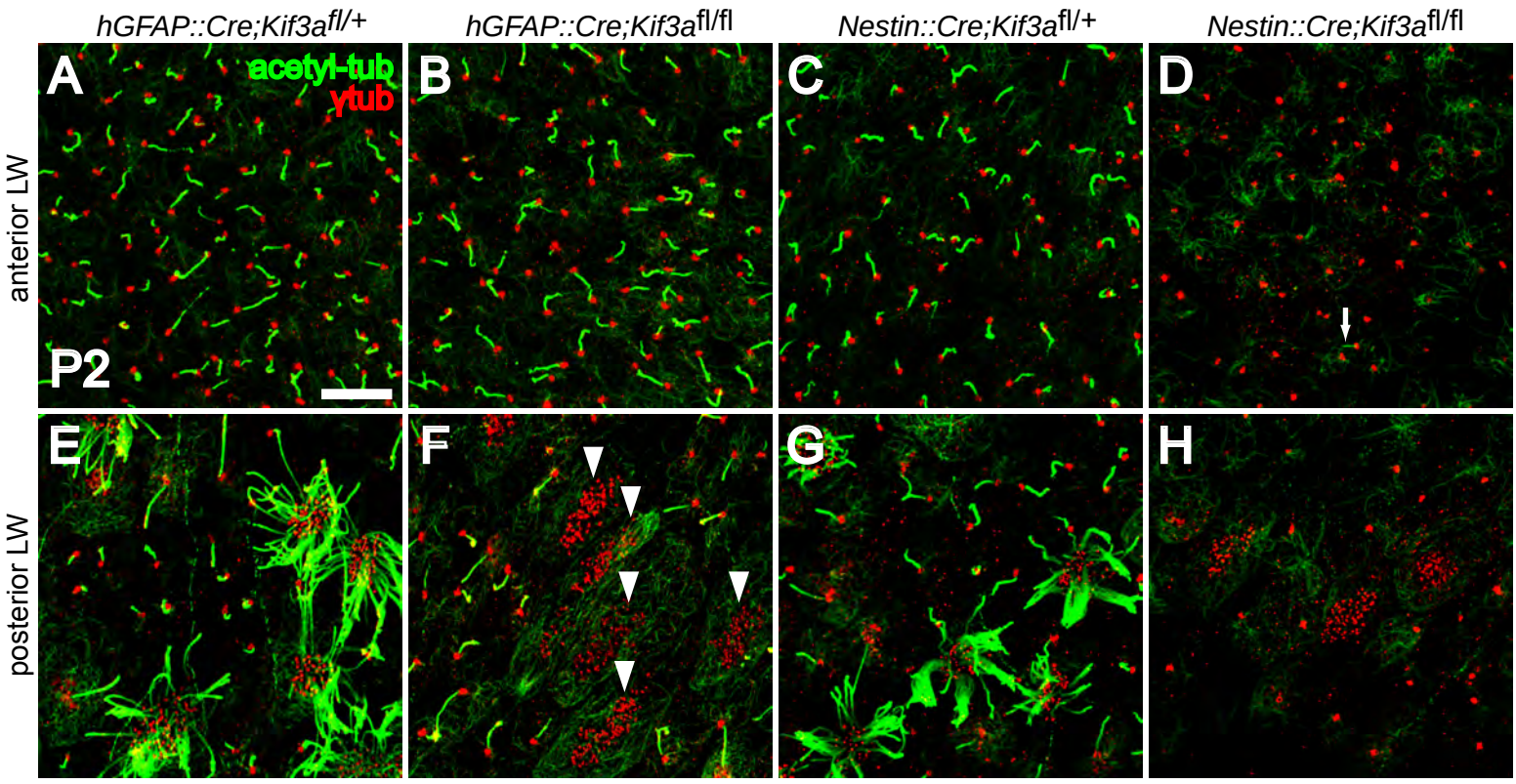

Figure S5. *hGFAP::Cre;Kif3a*$^{fl/fl}$ mutants lack motile cilia in ependymal cells but maintain primary cilia in radial glia while *Nestin::Cre;Kif3a*$^{fl/fl}$ mutants lack both sets of cilia. (**A-H**) Confocal images of anterior (A-D) and posterior (E-H) regions in lateral wall wholemounts stained for acetylated tubulin (green) and γ-tubulin (red) from P2 *hGFAP::Cre;Kif3a*$^{fl/fl}$ mutants (B, F), *Nestin::Cre;Kif3a*$^{fl/fl}$ mutants (D, H), and their respective control littermates (A, E, C, G). Basal body patches at the apical surface of *hGFAP::Cre;Kif3a*$^{fl/fl}$ mutant ependymal cells (arrowheads in F) did not have associated cilia, while in control ependymal cells (E) many long cilia were observed emanating from basal body patches. Nearly all radial glia in both controls and *hGFAP::Cre;Kif3a*$^{fl/fl}$ mutants had a primary cilium (A, B). In contrast, *Nestin::Cre;Kif3a*$^{fl/fl}$ mutants lacked both primary cilia in radial glial cells and motile cilia in ependymal cells (D, H). Arrow in D indicates trace acetylated tubulin in very rare cilia observed in these mutants. Scale bar = 10 um.

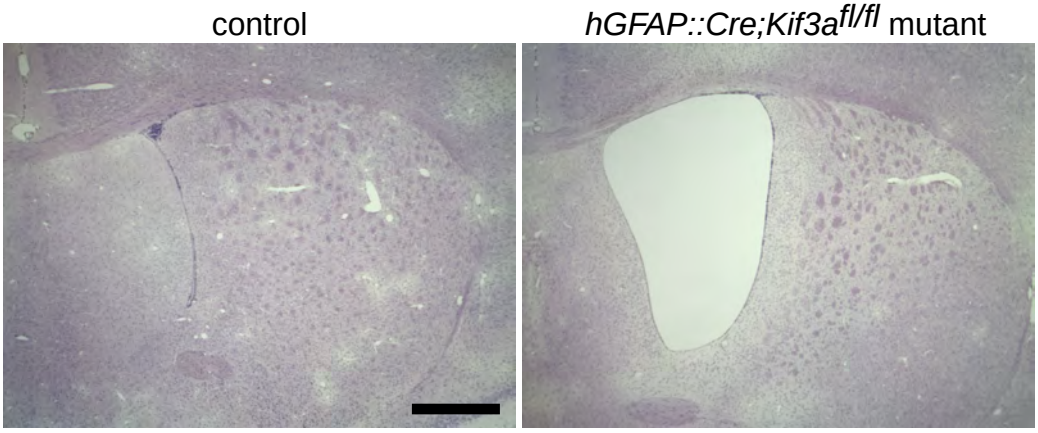

Figure S6. Hematoxylin-stained coronal sections from control and *hGFAP::Cre;Kif3a*$^{fl/fl}$ mutant mice demonstrate hydrocephalus in cilia-deficient mutants. Scale bar = 0.5 mm.

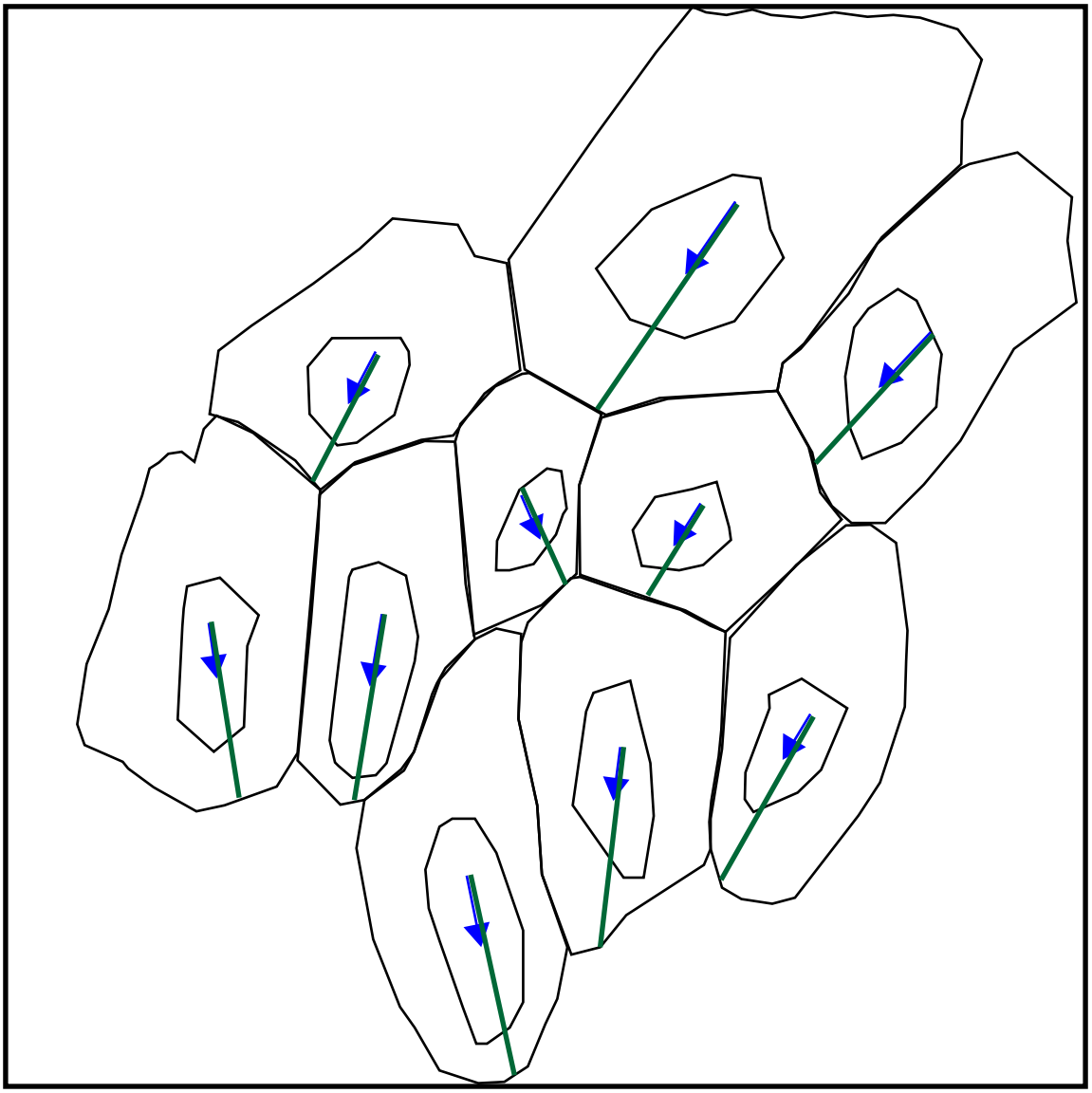

$$\frac{\text{magnitude of vector}}{\text{length of center-periphery line}} = \text{bb patch displacement}$$

Figure S7. Normalization of BB patch displacement to control for cell size and shape. The magnitude of the BB patch vector (blue arrow) was normalized by dividing by the length of the line (green line) drawn from the center of the apical surface, in the direction of the vector, to the cell perimeter. BB patch displacement was therefore represented as a ratio of the displacement along this line.

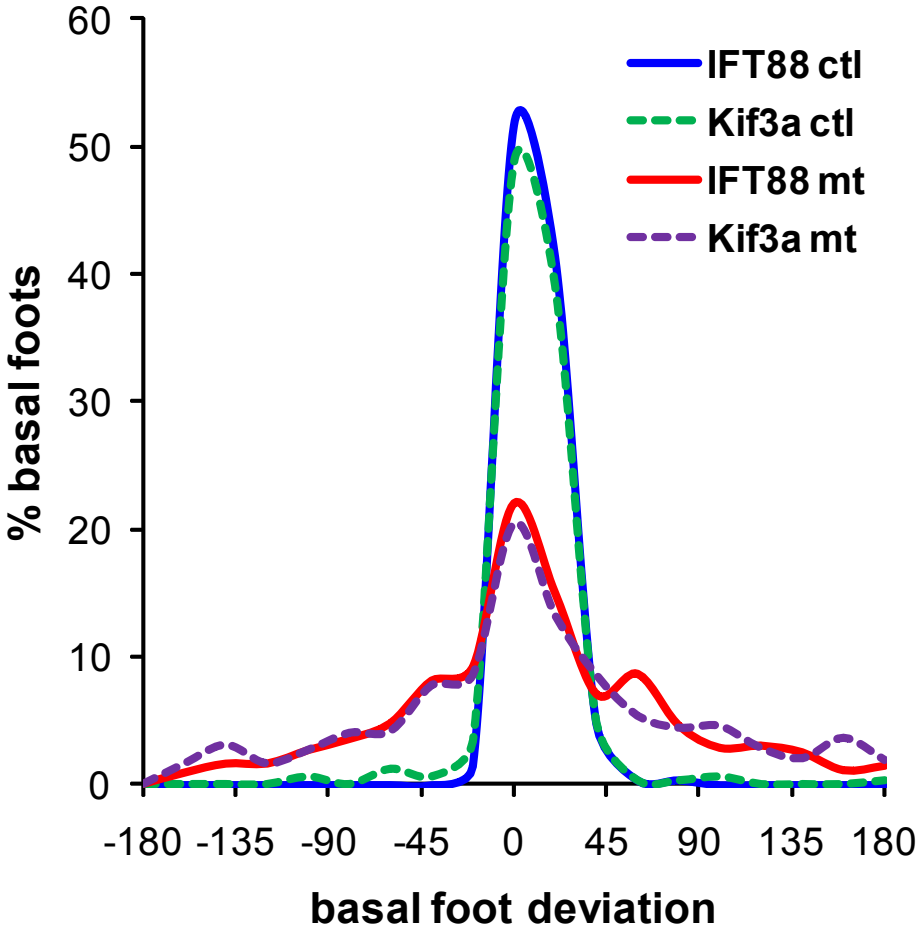

Figure S8. Histograms showing the distribution of basal foot angles around the median in control and *hGFAP::Cre;IFT88*$^{fl/fl}$ mutant ependyma (solid lines) compared to results from *hGFAP::Cre;Kif3a*$^{fl/fl}$ mutant animals and control littermates (dashed lines). This phenocopy confirmed that misalignment of basal body rotational orientation in mutant animals was due to defective ciliogenesis.

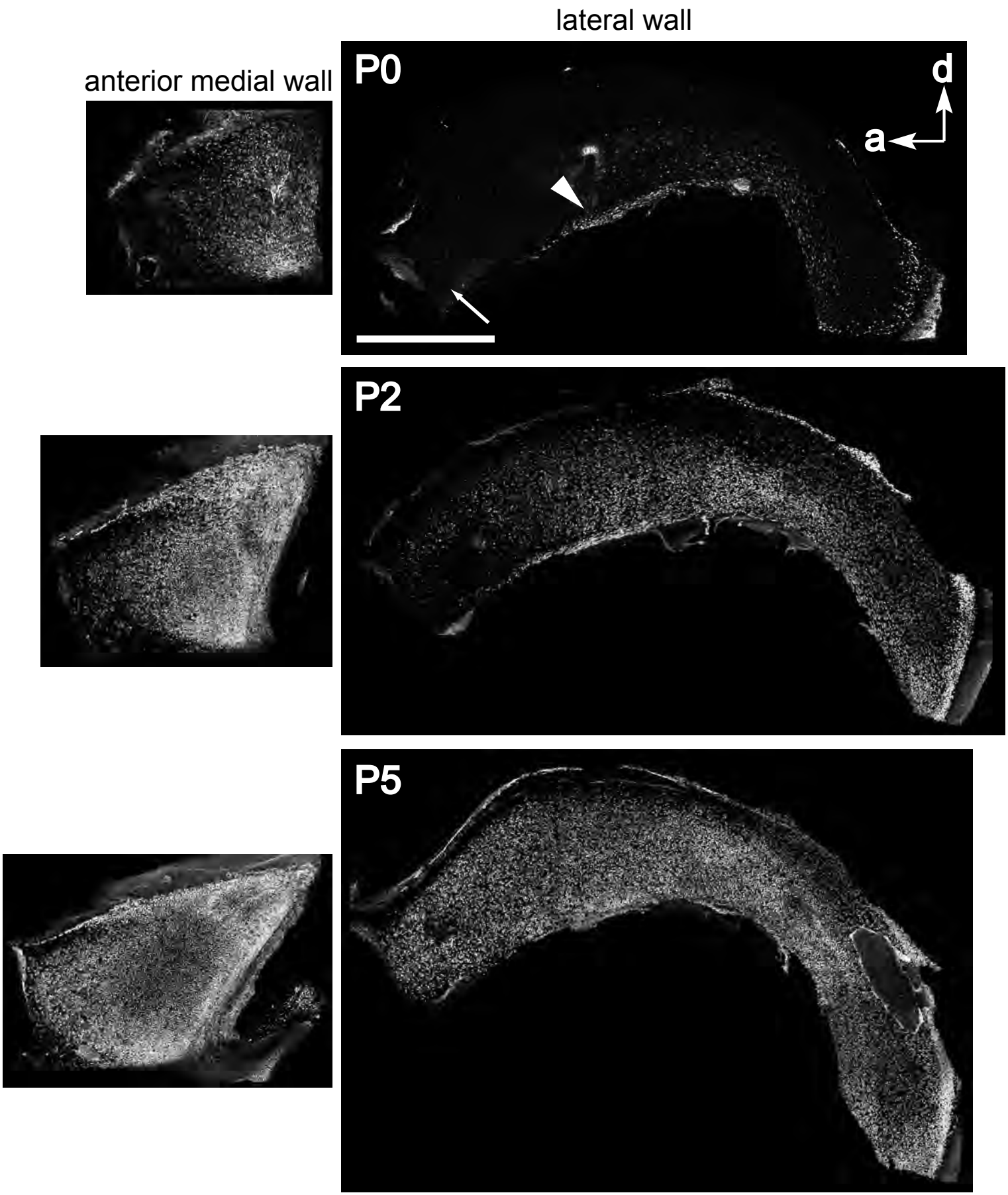

Figure S9. CD24 immunostaining on wholemounts reveals gradients of ependymal cell differentiation on the lateral and anterior medial wall of the LV in the early postnatal period. Ependymal differentiation proceeds from medial to lateral, posterior to anterior, and ventral to dorsal. Arrow indicates anterior region of lateral wall corresponding to where radial glial apical surfaces were analyzed in **Figure S10A**. Arrowhead indicates more posterior region where ependymal transformation has begun, corresponding to the transformation zone in **Figure S10B**. Anterior (a) and dorsal (d) directions are indicated by arrows in the upper right corner. Scale bar = 1 mm.

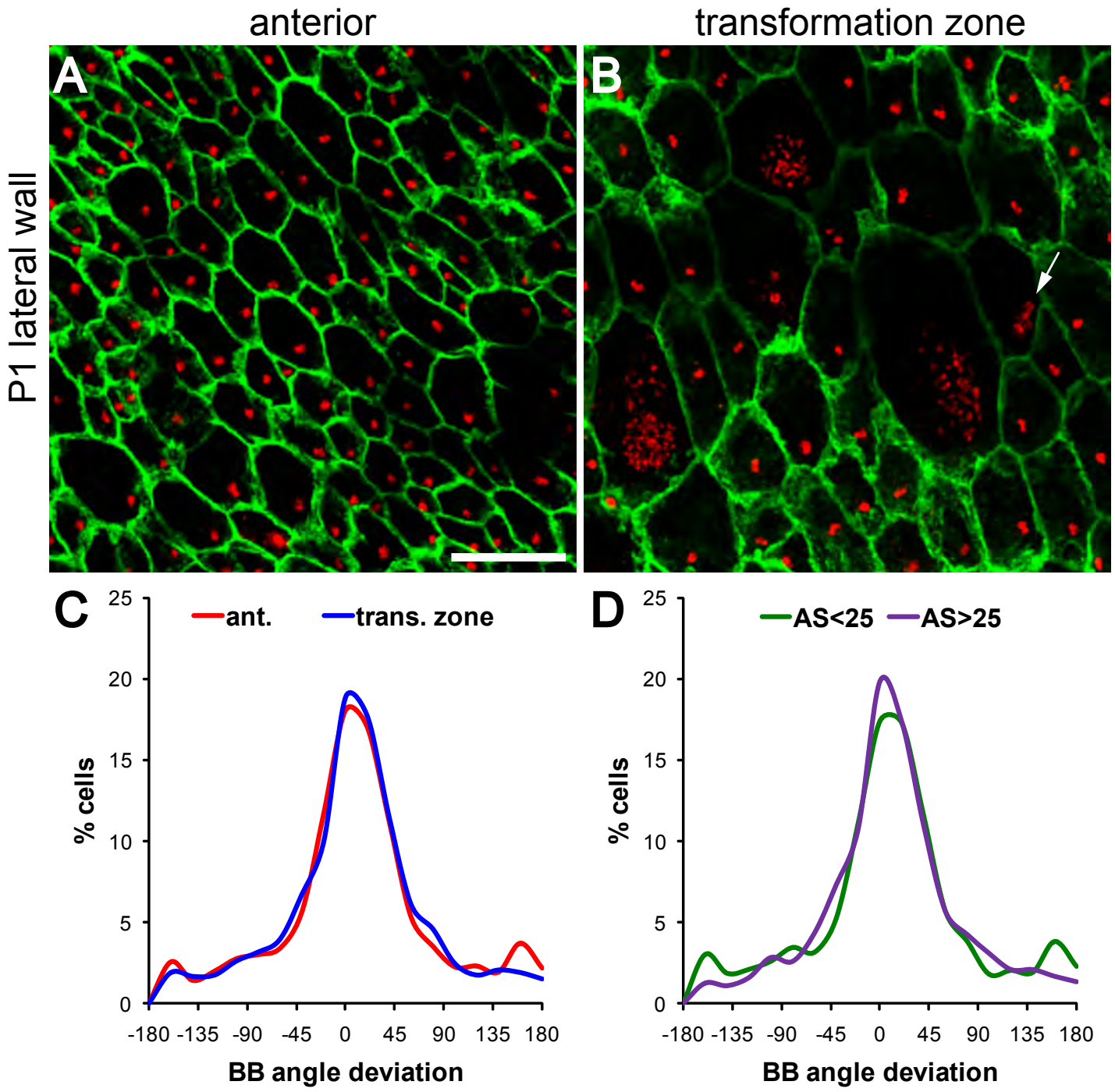

Figure S10. Planar polarity of basal body position in neonatal radial glia on the lateral wall.
(**A, B**) Confocal images of lateral wall wholemounts from P1 wild-type mice stained for β-catenin (green) and γ-tubulin (red). At this age, the anterior lateral wall (A) is covered by small apical surfaces of radial glia, whereas more posteriorly (B) radial glial apical surfaces have expanded and some radial glia have already transformed into ependymal cells with multiple basal bodies (regions analyzed shown in **Figure S9**). Note that some cells had deuterosomes stained by γ-tubulin (arrow in B). In both regions, neighboring cells had their basal body displaced to the ensuing "downstream" side of the cell with respect to CSF flow. Scale bar = 10 um.
(**C**) For each high power field analyzed, the difference between each cell's BB angle and the median BB angle in the field was calculated and this data was plotted on a histogram. Both regions analyzed displayed narrow distributions around 0°, which revealed that radial glia had planar polarized positioning of their basal body irrespective of their regional localization at P1.
(**D**) Subgrouping radial glia according to apical surface size (less than or more than 25 um^2) revealed that cells with small apical surfaces were well oriented. There is not a statistically significant difference between the two distributions shown (curve fit test, p=0.07).

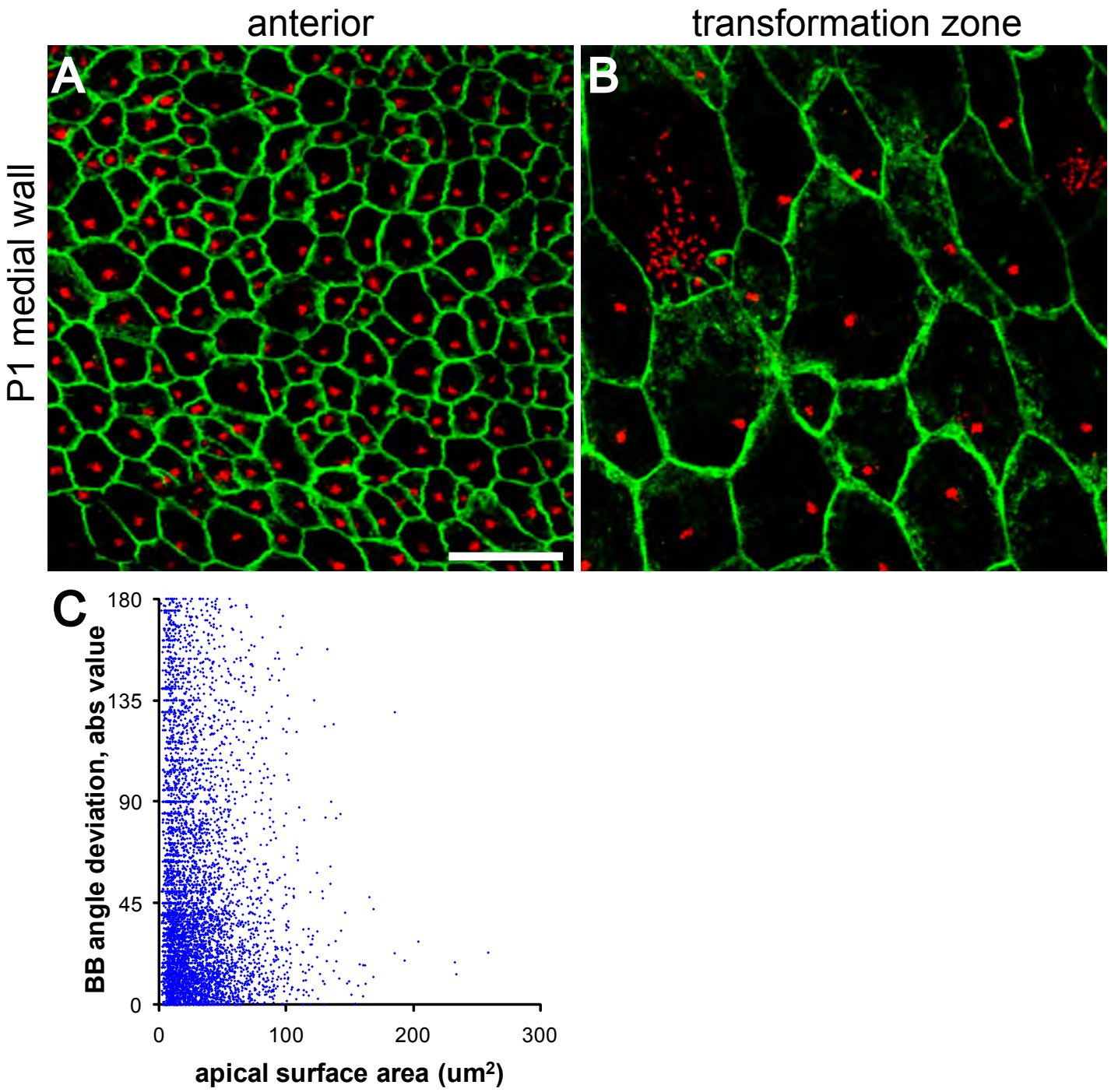

Figure S11. Planar polarity of basal body position in neonatal radial glia on the medial wall.
(**A, B**) Confocal images of medial wall wholemounts from P1 wild-type mice stained for β-catenin (green) and γ-tubulin (red). The anterior region (A) is covered by small apical surfaces of radial glia, whereas more posteriorly (B) radial glial apical surfaces have expanded and some radial glia have already transformed into ependymal cells with multiple basal bodies. In both regions, many cells had their basal body displaced to the ensuing "downstream" side of the cell with respect to CSF flow. Scale bar = 10 um.
(**C**) Scatter plot showing the relationship between the apical surface area of radial glial cells and the absolute value of their basal body angle deviation in the lateral and medial walls of the lateral ventricle.